Inorganic Chemistry

Article

pubs.acs.org/IC

Synthesis, Structural Characterization, and Physical Properties of the Early Rare-Earth Metal Digermanides $RE\mathrm{Ge}_{2-x}$ ($x \approx 1/4$) [*RE* = La−Nd, Sm]. A Case Study of Commensurately and Incommensurately Modulated Structures

Jiliang Zhang,[†] Paul H. Tobash,[†] William D. Pryz,[‡] Douglas J. Buttey,[‡] Namjung Hur,[§] Joe D. Thompson,[§] John L. Sarrao,[§] and Svilen Bobev*[,†]

[†]Department of Chemistry and Biochemistry and [‡]Department of Chemical Engineering, University of Delaware, Newark, Delaware 19716, United States

[§]Materials Science and Technology Division, Los Alamos National Laboratory, Los Alamos, New Mexico, 87544, United States

Supporting Information

ABSTRACT: Rare-earth metal germanides with the general formula $RE_4\mathrm{Ge}_7$ (*RE* = La, Ce, Pr, Nd, Sm) have been synthesized using the In-flux technique. Their structures have been established from single-crystal and powder X-ray diffraction, and the structural elucidation has been aided by electron diffraction. These compounds represent superstructures of the α-ThSi_2 structure type through the long- and/or short-range vacancy ordering. $RE_4\mathrm{Ge}_7$ (*RE* = Pr, Nd, Sm) appear to be commensurately modulated 4-fold superstructure of $RE\mathrm{Ge}_{2-x}$ (x = 1/4), while coexistence of commensurate and incommensurate modulation is revealed in the La- and Ce-analogues. These results shed more light on the structural evolution of the $RE\mathrm{Ge}_{2-x}$ phases as function of the vacancy concentration and nature of the rare-earth metal. Measurements of the magnetic susceptibilities on well-characterized single-crystals show ferromagnetic, antiferromagnetic, and even spin-glass-like behaviors. Mean-field theory is used to evaluate the correlations between structural and magnetic property data. Measurements on the electrical resistivities and the heat capacities are also presented and discussed.

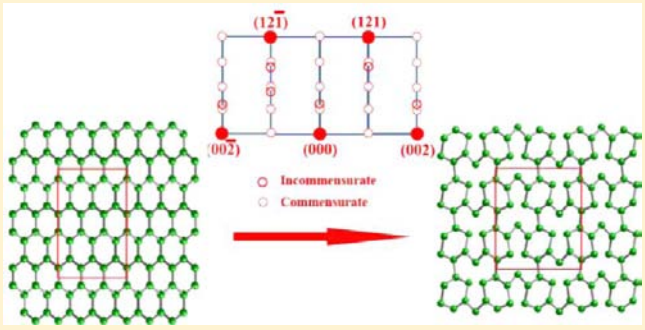

INTRODUCTION

Rare-earth metal germanides with general formula $RE\mathrm{Ge}_{2-x}$ ($0.5 < x \leq 0$) have been known for a very long time, and have been intensively studied because of their rich structural chemistry and interesting properties.[1−3] Such compounds are excellent candidates for case studies on structure−property relationships because they exist as virtually continuous series throughout the lanthanide family. The two common structure types adopted by the $RE\mathrm{Ge}_{2-x}$ compounds are the α-ThSi_2 (space group $I4_1/amd$),[2b] and the AlB_2 (space group $P6/mmm$) structure types.[1d,e] It has been shown that the realization of a given structure is largely dependent on the nature (i.e., size) of the rare-earth metal. For example, the early lanthanides (largest atomic size) predominantly form with the α-ThSi_2 structure type;[2b] a gradual transition to an orthorhombically distorted structure (i.e., α-GdSi_2 structure type, space group *Imma*) is concomitant with the decrease of the atomic size on moving to the middle of the 4f-block.[1g] The hexagonal AlB_2 structure is prevalent for the late lanthanides (smallest atomic size). Additionally, the structural variations are also governed by the degree of substoichiometry: the $RE\mathrm{Ge}_{2-x}$ phases with the α-ThSi_2 structure are generally with the lowest concentration of vacancies ($x \approx 0$),[2b] while higher rates of Ge-deficiency ($x \approx$ 0.4−0.5) seems to be favored by the compounds with the AlB_2-type structure.[1d,e]

The above classification and description, however, is an oversimplification and should be used with caution—in most $RE\mathrm{Ge}_{2-x}$ compounds, partial or full ordering of the vacancies is observed, giving rise to a multitude of superstructures. Phase transitions between polymorphs and intricate interplay between thermodynamic and metastable (kinetic) phases are also frequently reported.[3,4] In this sense, it is not surprising that often, one can find significant differences between the properties of samples with structures and compositions, presumed to be a match to one another.[2a] Such structural nuances are hard to distinguish based on routine X-ray diffraction work and some of the misinterpreted data have propagated in the literature; erroneous information can be found even in the current binary phase diagrams.[5] Therefore, resolving of the "known" structures in greater detail and revisiting the synthetic routes is becoming an important issue.

Received: October 4, 2012
Published: January 8, 2013

Recent results, including work from our laboratories, have shown that better control over the reaction outcome can be achieved using the flux-growth method,[6] and that the grown single-crystals are not statistically disordered $RE\mathrm{Ge}_{2-x}$ but rather stoichiometric $RE_3\mathrm{Ge}_5$[4] and $RE_4\mathrm{Ge}_7$[7] compounds with structures that exhibit long-range vacancy ordering. The germanides with the formula $RE_3\mathrm{Ge}_5$ (i.e., $RE\mathrm{Ge}_{2-x}$ with x = 1/3) adopt at least 3 different structures[4,8] related to both the α-ThSi_2 and the AlB_2 structure types; they form with many different rare-earth metals, ranging from Nd to Yb.[9] An ordered superstructure for ErGe_{2-x} with x = 1/2 has also been recently reported.[10] The $RE_4\mathrm{Ge}_7$ germanides (i.e., $RE\mathrm{Ge}_{2-x}$ with x = 1/4) are relatively uncommon and had been known only for Nd;[7a] the structure of the Pr analogue was published not long ago, while this work was in still progress.[7b]

With this paper, we report the results from our detailed investigations on the series of $RE_4\mathrm{Ge}_7$ (RE = La–Nd, Sm) compounds. While the structures of $RE_4\mathrm{Ge}_7$ (RE = Pr, Nd, Sm) could be established from single-crystal X-ray diffraction data as commensurate superstructures of the α-ThSi_2 type, the structures of $\mathrm{La}_4\mathrm{Ge}_7$ and $\mathrm{Ce}_4\mathrm{Ge}_7$, on the other hand, could not be satisfactorily elucidated from X-ray work alone. More structural details were extracted using electronic diffraction and transmission electron microscopy. Also reported are the magnetic susceptibilities, specific heats, and electrical resistivities of all of the title compounds, measured on single-crystals.

EXPERIMENTAL SECTION

Synthesis. All manipulations were performed inside an argon-filled glovebox with controlled oxygen and moisture levels below 1 ppm or under vacuum. The starting materials, rare-earth metals (pieces, purity >99.9% metal basis, purchased from Ames Laboratory or Alfa-Aesar), Ge (lump, purity 99.999%, Acros), and In (shot, purity 99.99%, Alfa-Aesar) were used as received. The reactions were carried out in alumina crucibles (2 cm^3), which were subsequently enclosed in fused silica ampules and flame-sealed under vacuum. Stoichiometric reactions in welded Nb tubes were also pursued but they always yielded inhomogeneous products.

$\mathrm{Sm}_4\mathrm{Ge}_7$ was the first of the title compounds that was serendipitously identified as one of the products of a reaction aimed at $\mathrm{Sm}_2\mathrm{InGe}_2$.[6c] As described in detail elsewhere, all reactions with the mid-to-late rare-earth metals with elemental ratio RE:In:Ge = 1:10:1 (RE = Sm, Gd–Yb) afforded crystals of the $RE_2\mathrm{InGe}_2$ compounds; reactions with Sm, in addition to $\mathrm{Sm}_4\mathrm{Ge}_7$ and $\mathrm{Sm}_2\mathrm{InGe}_2$, also produced $\mathrm{Sm}_3\mathrm{Ge}_5$, and SmIn_3.[6c] Similar reactions with the early rare-earth metals RE = La, Ce, Pr, and Nd resulted in the binary phases $RE\mathrm{In}_3$ as main phases.[6c] This is suggestive of a brake point in the periodicity among the lanthanide elements, which was further confirmed by setting a different batch of reactions, which were loaded with the ratio RE:In:Ge = 1:10:2 and subjected to the same heating conditions as before: quick heating (rate 300 K/h) to 1373 K, homogenization at this temperature for 1.5–3 h, followed by a cooling to 673 K over a period of 20 h. The excess molten In (mp 430 K)[11] was then removed by centrifugation. The outcomes of these experiments were large (up to 4–5 mm in size) plate-like crystals of $RE_4\mathrm{Ge}_7$, as well as a few Ge and $RE\mathrm{In}_3$ (RE = La–Nd, Sm) crystals, easily conspicuous by their cubic morphology. The corresponding reactions with the late rare-earth metals did not afford any of these phases.

The crystals of the title compounds display silver–metallic luster, which does not deteriorate in air over periods greater than 1 year. The materials also appear to be resistive to dilute hydrochloric acid solutions, therefore, 1 M HCl was used to remove the traces of In, which remained adhered to the surface of the crystals (prior to property measurements).

X-ray Powder Diffraction. X-ray powder diffraction patterns were taken at room temperature on a Rigaku MiniFlex powder diffractometer using filtered Cu Kα radiation. The intensities and the positions of the experimentally observed peaks and those calculated based on the corresponding single-crystal structures matched very well to one another. Representative X-ray powder diffraction patterns are provided in Supporting Information, Figures 1S and 2S.

Single Crystal X-ray Diffraction. Crystals were selected from the reaction products and were cut under a microscope to about 0.07–0.08 mm in all dimensions. They were placed on glass fibers using Paratone N oil. Intensity data sets were collected at 120 K on a Bruker SMART CCD-diffractometer equipped with monochromated Mo Kα radiation. The data collection routine in SMART[12] with scans at different ω and ϕ angles allowed for full coverage of the reciprocal space up to $\sin\theta/\lambda \approx 0.75$ $\mathrm{Å}^{-1}$. The collected frames were integrated using the SAINTplus program.[13] SADABS was used for semiempirical absorption correction based on equivalents.[14] The SHELX software package[15] was used to solve the structures by direct methods; structure refinements were carried out by full-matrix least-squares methods on F^2.

Several observations with regards to the single-crystal X-ray diffraction studies deserve a special mention. First, indexing the diffraction data using the strong reflections was trivial: the structures could be readily solved and refined as defect versions of the α-ThSi_2 structure (i.e., as $RE\mathrm{Ge}_{2-x}$ ($x \approx 1/4$)). Some details on representative structural refinements in the tetragonal $I4_1/amd$ space group of the archetype with unit cell constants $a \approx 4.17$–4.38 Å and $c \approx 13.79$–14.23 Å are given in Supporting Information, Table S6. However, the poor residuals along with the abnormal anisotropic displacement parameters were among some of the indications that the selected model was not adequate. Second, reduction of the symmetry to orthorhombic and assuming the GdSi_2 type (a slightly distorted version of the same structure, which is described by two independent Ge sites in space group $Imma$) resulted in similar problems—they are best illustrated on example of LaGe_{2-x} ($a \approx 4.30$ Å; $b \approx 4.40$ and $c \approx 14.16$ Å)—as shown in Supporting Information, Table S7. Third, the fact that there were many weak reflections that were violations of the chosen symmetry, but could be indexed with different orthorhombic unit cells, 4 times larger, was a clear indication that the atomic structure is a better fit to the known $\mathrm{Nd}_4\mathrm{Ge}_7$[7a] structure type (with the orthorhombic $C222_1$ space group). Such conclusion could be corroborated by the single-crystal X-ray diffraction work for $RE_4\mathrm{Ge}_7$ (RE = Pr, Nd, Sm); Table 1 gives a summary of the structure refinement parameters for $\mathrm{Sm}_4\mathrm{Ge}_7$.

For the La- and Ce-analogues, all attempts to resolve the structure from the gathered single-crystal X-ray diffraction data were unsuccessful. This work led to unsatisfactory residuals and abnormally elongated thermal parameters in any of the three structural models. The deficiencies of these trial refinements are suggestive of the vacant

Table 1. Selected Crystallographic Data for $\mathrm{Sm}_4\mathrm{Ge}_7$

	$\mathrm{Sm}_4\mathrm{Ge}_7$
formula weight	1109.53
temperature (K)	120(2)
radiation	Mo Kα, λ = 0.71073 Å
space group	$C222_1$, Z = 4
a (Å)	5.892(2)
b (Å)	13.781(5)
c (Å)	11.792(5)
V ($\mathrm{Å}^3$)	957.6(6)
ρ_{cal} (g cm^{-3})	7.696
μ (cm^{-1})	456.41
final residuals ($I > 2\sigma_I$)[a]	R_1 = 0.0345/wR_2 = 0.0839
final residuals (all data)[a]	R_1 = 0.0384/wR_2 = 0.0864
largest diff. peak/hole (e^- $\mathrm{Å}^{-3}$)	2.56/−2.52

[a] $R_1 = \sum||F_o| - |F_c||/\sum|F_o|$, $wR_2 = \{\sum[w(F_o^2 - F_c^2)^2]/\sum[w(F_o^2)^2]\}^{1/2}$, where $w = 1/[\sigma^2F_o^2 + (0.036{\cdot}P)^2 + 13.79{\cdot}P]$, and $P = (F_o^2 + 2F_c^2)/3$.

dx.doi.org/10.1021/ic3021645 | Inorg. Chem. 2013, 52, 953–964

Ge sites in the crystal structure being poorly ordered. Long exposure zone-images (300−1800 s), taken on the CCD-diffractometer did not show any "streaking" or other problems due to lack of order, but credible superstructure reflections were not apparent (see Supporting Information). The search for possible (in)commensurate modulation is addressed later on in the transmission electron microscopy part of this paper. Yet, the disorder could not be completely resolved; for the sake of simplicity, we have dubbed these phases as La_4Ge_7 and Ce_4Ge_7 and report them as "averaged" 4-fold superstructures of the α-$ThSi_2$ type.

Final positional and equivalent displacement parameters are given in Table 2 along with interatomic distances in Table 3. The

Table 2. Atomic Coordinates and Equivalent Isotropic Displacement Parameters (U_{eq}[a]) of Sm_4Ge_7

atom	site	x	y	z	U_{eq} (Å^2)
Sm1	8c	0.2624(1)	0.2454(1)	0.1198(1)	0.005(1)
Sm2	4b	0	0.0041(1)	1/4	0.005(1)
Sm3	4a	0.5132(2)	0	0	0.005(1)
Ge1	8c	0.4822(3)	0.5886(1)	0.0107(1)	0.010(1)
Ge2	8c	0.2526(3)	0.1726(1)	0.3719(1)	0.009(1)
Ge3	8c	0.1735(3)	0.3525(1)	0.3373(2)	0.015(1)
Ge4	4b	0	0.5611(2)	1/4	0.009(1)

[a] U_{eq} is defined as one-third of the trace of the orthogonalized U_{ij} tensor.

Table 3. Selected Interatomic Distances in Sm_4Ge_7

atom pair	distance (Å)	atom pair	distance (Å)
Ge1−Ge1	2.457(3)	Sm1−Ge2	3.136(2)
Ge1−Ge2	2.560(2)	Sm1−Ge2	3.137(2)
Ge1−Ge3	2.679(2)	Sm1−Ge2	3.198(2)
Ge2−Ge3	2.556(3)	Sm1−Ge4	3.282(2)
Ge2−Ge4	2.560(2)	Sm2−Ge3 × 2	3.021(2)
Ge2−Ge1	2.560(2)	Sm2−Ge4 × 2	3.049(2)
Ge3−Ge2	2.556(3)	Sm2−Ge1 × 2	3.100(2)
Ge3−Ge1	2.679(2)	Sm2−Ge2 × 2	3.110(2)
Ge4−Ge2 × 2	2.560(2)	Sm2−Ge1 × 2	3.289(2)
Sm1−Ge3	3.004(2)	Sm3−Ge3 × 2	3.004(2)
Sm1−Ge3	3.005(2)	Sm3−Ge4 × 2	3.067(2)
Sm1−Ge1	3.019(2)	Sm3−Ge2 × 2	3.138(2)
Sm1−Ge1	3.025(2)	Sm3−Ge1 × 2	3.167(2)
Sm1−Ge2	3.030(2)	Sm3−Ge1 × 2	3.217(2)

crystallographic information file (CIF) has also been deposited with Fachinformationszentrum Karlsruhe [76344 Eggenstein, Leopoldshafen, Germany; fax: (49) 7247−808−666; email: crysdata@fiz.karlsruhe.de; depository number CSD-424989 (Sm_4Ge_7)].

Transmission Electron Microscopy. Microscopy studies were done at the W. M. Keck Electron Microscopy Facility in the College of Engineering at the University of Delaware. Selected-area electron diffraction (SAED) data were gathered using a JEOL 2000FX Transmission Electron Microscope (TEM), operated at 200 keV using a camera length of 80 cm and acquisition times between 60 and 90 s. All samples for TEM were prepared by first grinding the crystals, suspending the powder in ethanol, and applying 1−2 drops of solution to a 200- or 300-mesh Cu grid coated with a lacey-carbon film. Such procedure is not expected to introduce structural faults (or variations) because of the brittleness of the samples.

Physical Properties. Field-cooled (FC) and zero field-cooled (ZFC) DC magnetization (M) measurements were completed using a Quantum Design MPMS SQUID magnetometer in the temperature range 5−350 K and in an applied fields of 100 or 1000 Oe. For all of these measurements the samples were secured in a custom-designed low background sample holder. The raw magnetization data were corrected for the holder contribution and converted to molar susceptibility ($\chi_m = M/H$). Field dependent measurements at 2 K and in applied fields up to 50 kOe were also completed for some of the compounds. The specific heat data were measured in a He4 cryostat using the thermal relaxation method within the temperature range 2−250 K. The electrical resisitivity measurements were done using the four-probe technique from 2 to 300 K with an excitation current of 1 mA. The ohmic contacts were made by placing 0.001 in. platinum wires along with silver epoxy to the smooth faces of the crystals. All measurements were taken along the direction of the plates.

RESULTS AND DISCUSSION

Synthesis, Structure, and Bonding. The structures of three of the five title compounds were elucidated by X-ray diffraction—RE_4Ge_7 (RE = Pr, Nd, Sm). Nd_4Ge_7 is the archetype, and its structure has been known since 1999;[7a] Pr_4Ge_7 was reported while this work was ongoing.[7b] Sm_4Ge_7 is a newly identified binary phase, isotypic with the former two. While the La- and Ce compounds were synthesized in analogous fashion and appear to have similar compositions as RE_4Ge_7 (RE = Pr, Nd, Sm), their structures are subtly different. Noteworthy, none of the RE-Ge (RE = La, Ce, Pr, Nd, Sm) phase diagrams[5] shows any hints for the existence of binary phases at 63.6 at.% Ge. For example, in the composition range from about 60 at.% Ge to 62.6 at.% Ge of the established phase diagrams, several phases are specified: (1) α-$REGe_{2-x}$ (low temperature form, $GdSi_2$ type, $Imma$ space group) and (2) β-$REGe_{2-x}$ (high temperature form, α-$ThSi_2$ type, $I4_1/amd$ space group). In the case of the Sm−Ge diagram, a third $REGe_{2-x}$ phase at about 60 at.% Ge has been ascribed to the AlB_2 type ($P6/mmm$ space group). Our recent studies have shown that in the latter case, there are α-Sm_3Ge_5 (low temperature form, $Fdd2$ space group) and β-Sm_3Ge_5 (high temperature form, $P\bar{6}2c$ space group) at exactly 62.5 at.% Ge; now, we provide evidence for yet another "missed" compound in this system.

The crystal structure of Sm_4Ge_7 is depicted in Figure 1. It can be described as a three-dimensional (3D) polyanionic network of 2- and 3-bonded Ge atoms with the rare-earth metal cations occupying the channels created within the anionic substructure. The structure is clearly a close relative to the α-$ThSi_2$ type,[16] from which it can be conveniently derived. The Ge-network in the latter is essentially two zigzag chains which propagate in

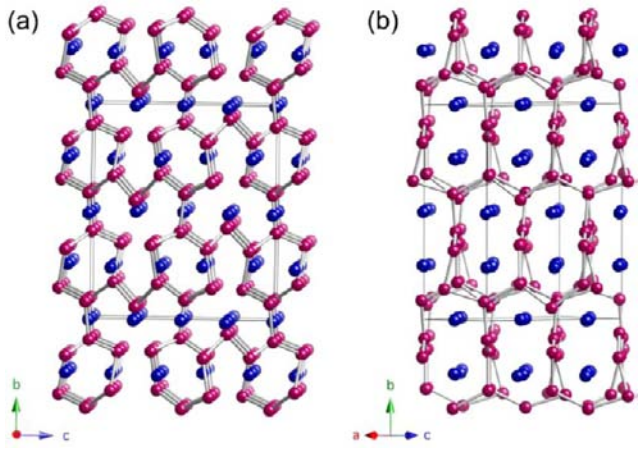

Figure 1. (a) Orthorhombic crystal structure of Sm_4Ge_7, viewed down the a-axis. (b) The Sm_4Ge_7 structure, projected orthogonally to the [201] plane (emphasizing the relationship to the α-$ThSi_2$ structure). Sm atoms are shown as dark-blue spheres, the Ge atoms are drawn as maroon spheres, respectively. The unit cell is outlined.

dx.doi.org/10.1021/ic3021645 | Inorg. Chem. 2013, 52, 953−964

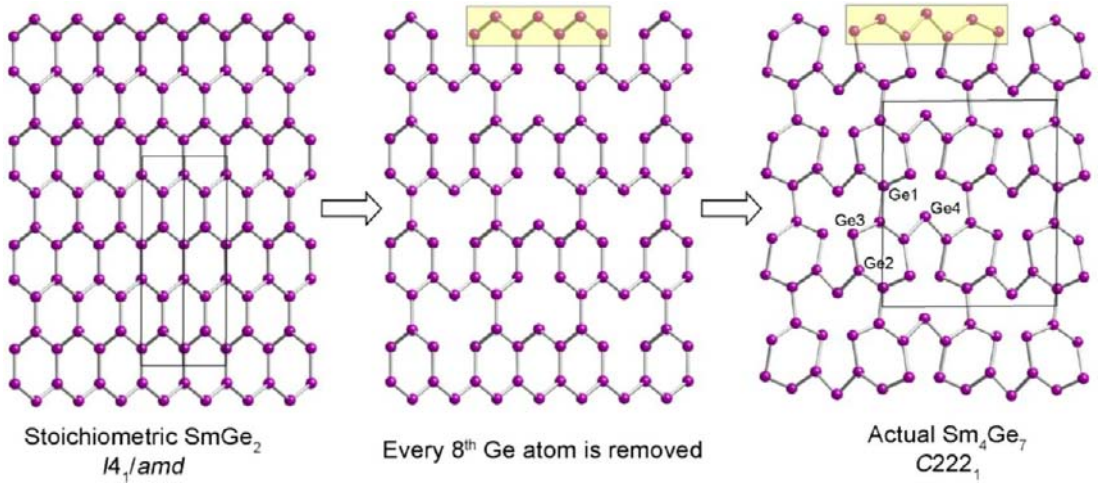

Figure 2. Schematic representation of the relation between the idealized $SmGe_2$ structure (α-$ThSi_2$ structure type) and the observed Sm_4Ge_7 structure. The Ge_7 fragments, created through the removal of every 8th Ge-atom from two mutually perpendicular chains are emphasized. The vacancy and the concomitant distortion alleviate the unfavorable "sp^2-hybridization" in the parent zigzag chains.

orthogonal directions; in the former, the Ge-network is built from Ge_7 fragments, which are cut-outs from the same zigzag chains, where every eighth Ge-atom is missing (Figure 2). In this way, the anionic substructure can also be viewed as an arrangement of slightly distorted 12-membered and 6-membered helical channels. Shorter 5-atom remnants of intersecting zigzag Ge chains are seen in the orthorhombic structure of Sm_3Ge_5,[4a] where only the 12-membered "cookie-cutters" are present. Therefore, a direct comparison between the structures and the chemical bonding of Sm_4Ge_7 and Sm_3Ge_5 will be instructive, and will be discussed in the following paragraphs.

In Sm_4Ge_7, there are four independent Ge-sites in the asymmetric unit (Table 2); the Ge−Ge interatomic distances are given in Table 3. The average of the Ge−Ge distances (ca. 2.56 Å) is comparable to the Ge−Ge distances in Sm_3Ge_5[4a] (2.543−2.558 Å) and $EuGe_2$ (2.565 Å),[1c] among others. However, we must note the somewhat large spread and the fact that the shortest Ge1−Ge1 distance (2.457(3) Å) matches almost exactly the Ge−Ge distances in elemental Ge,[16] which is unusual for a structure where the Ge atoms are expected to be in a formally reduced state, but is not without a precedent.[4] This bond serves to connect together the hexagonal channels in the structure. The longest Ge−Ge distance (2.679(2) Å), on the other hand, occurs adjacent to the shortest one in a nearly orthogonal direction; its value is greater than the typical values and matches the distances found in the *RE*Ge monogermanides with the FeB and CrB type (ca. 2.65 Å on average),[16,17] as well as RE_3Ge_4 (2.575−2.657 Å).[18]

It should also be noted that the Ge−Ge distances resulting from the refinements of the structures using the subcell models either with the *Imma* or $I4_1/amd$ space groups led to unreasonably short distances on the order of about 2.2−2.3 Å (Supporting Information, Table S3) and with Ge−Ge−Ge angles on the order of 120°. Apparently, it is through the vacancy ordering and the shifting of the Ge atoms surrounding the vacant site, which allow the structure to "relax" (as shown in Figure 2), leading to more reasonable bond distances and corresponding bond angles on the order of 93.60−135.80°. Thereby, the imposed "sp^2-hybridization" of the Ge atoms in the subcell models is alleviated. Very similar metrics for the bond angles are observed in the Ge_5 fragments of Sm_3Ge_5 as well.[4a]

The Ge−Ge distances among the three members of the RE_4Ge_7 family (Table 3, and Supporting Information, Tables S3 and S4 for the bond distances in Pr_4Ge_7 and Nd_4Ge_7, respectively) show correlation with the lanthanide contraction. The contacts between the rare-earth metal and the germanium atoms range from about 3.0 to about 3.3 Å (Table 3) and are also comparable to those in the *RE*Ge monogermanides.[16,17] These values are also on par with the sum of the corresponding Pauling radii.[19] The coordination spheres of the three crystallographically independent Sm atoms are irregular polyhedra of 9 or 10 next-nearest Ge atoms, as shown in Figure 3.

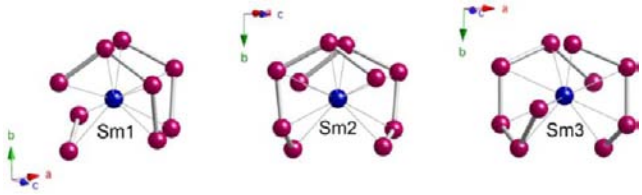

Figure 3. Coordination polyhedra of the Sm atoms in Sm_4Ge_7.

As noted already, the Ge substructure in Sm_4Ge_7 can be derived from that of $SmGe_2$ (space groups $I4_1/amd$ or *Imma*) through the removal of every eighth Ge atom in the chains, which leaves behind the 7-membered fragments. The unit cell transformation from the α-$ThSi_2$ type tetragonal cell (a = 4.1692(6) Å, c = 13.790(4) Å) to the orthorhombic cell (a = 5.892(2) Å, b = 13.781(5) Å, c = 11.792(5) Å) is shown in Figure 4a.

As depicted, the diagonal of the tetragonal cell becomes the a_o lattice parameter in the new supercell ($a_t \times \sqrt{2}$); the c_o lattice parameter in the supercell is effectively the addition of two square diagonals ($2a_t \times \sqrt{2}$); and the b_o lattice parameter is unchanged from the c_t. This unit cell transformation leads to a four times larger unit cell, whereby all sites are crystallographically ordered. Similar crystallographic transformations can be found for $SmGe_{2-x}$ (x = 1/3), that is, for the case where every sixth Ge atom is missing, as shown in Figure 4b. The

dx.doi.org/10.1021/ic3021645 | *Inorg. Chem.* 2013, 52, 953−964

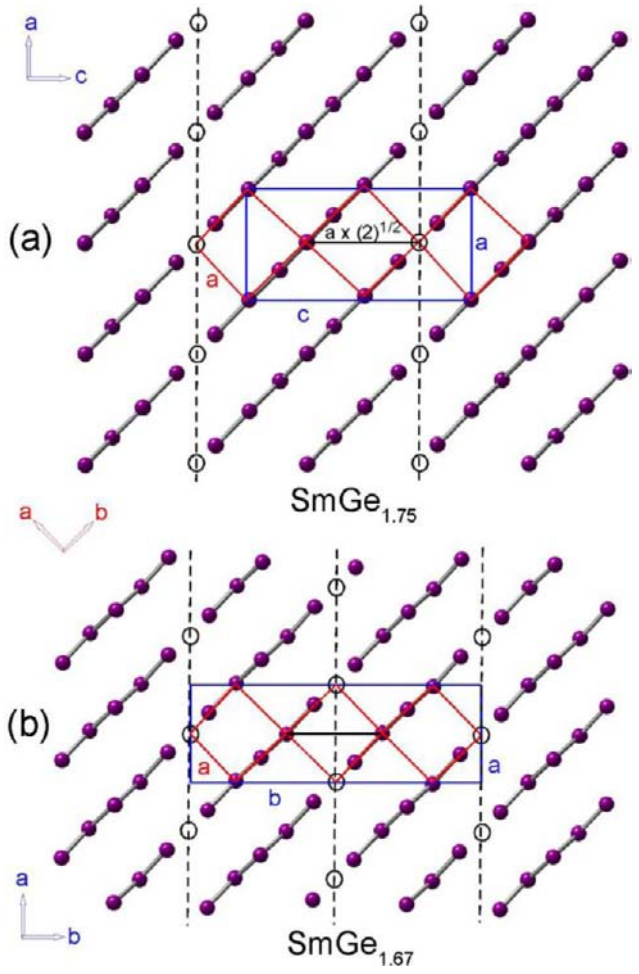

Figure 4. (a) Schematic representation of the crystallographic relationship between the Ge substructure in Sm_4Ge_7 ($SmGe_{1.75}$) in space group $C222_1$ and that in the hypothetical compound $SmGe_2$ (α-$ThSi_2$ type, space group $I4_1/amd$). Every eighth Ge atom in the parallel chains is missing in an ordered fashion (empty circles), leaving behind 7-membered fragments. (b) The crystallographic relationship between the Ge substructure in Sm_3Ge_5 ($SmGe_{1.67}$) in space group $Fdd2$ and that in $SmGe_2$. Here, every sixth Ge atom is missing, leaving behind 5-membered fragments. The axes shown in red refer to the orientation of the subcells, and in blue, to the orientation of the supercells, respectively.

long-range vacancies order is apparent for the Pr, Nd, and Sm compounds, while the La and Ce analogues are showing only short-range ordering: the difference in the structures can be most likely attributed to the larger size of the rare-earth metal.

This brings us to the discussion of the La_4Ge_7 and Ce_4Ge_7 structures. As described in the experimental section, the single-crystal X-ray diffraction work led to unsatisfactory refinements using the same model as that applied for the RE_4Ge_7 (RE = Pr, Nd, Sm): selected refinement parameters for the Ce_4Ge_7 structure are gathered in Supporting Information, Table S5. Initially it was thought that this could be an artifact from poor crystallinity, so attempts to improve the single-crystal quality through 2-weeks of annealing at temperatures between 500 and 600 °C were undertaken. Subsequently, the crystal quality proved not be an issue, yet we were unsuccessful in the efforts to pin down the anticipated long-range ordered superstructure from X-ray diffraction work. Possible flux inclusions could also be ruled out, since there was no evidence for it in the $PrGe_{2-x}$, $NdGe_{2-x}$ or $SmGe_{2-x}$ specimens; more importantly, crystals obtained by direct fusion of La (or Ce) and Ge in welded Nb-tubes also exhibited similar anomalies. In all cases, the refinements did not show any improvement over the substructure model (space groups $I4_1/amd$ or $Imma$), and led to hugely elongated thermal parameters for the Ge atoms, and very poor residuals.

It is also important to note the poor reproducibility: single-crystal study on a different crystal from another batch suggested a smaller degree of orthorhombicity: cell parameters a = 4.274(3) Å, b = 4.387(3) Å, c = 14.079(10) Å. These values are not comparable with those reported by Guloy and Corbett for their $LaGe_{2-x}$ single-crystal refinement: a = 4.2680(7) Å, b = 4.2735(6) Å, and c = 14.404(1) Å.[1a] The discrepancy is likely due to the variations in the distributions of the vacant sites within the orthogonal chains. Powder X-ray diffraction patterns also exhibited noticeable splitting of some of the strong peaks between 20° and 45° in 2θ (Supporting Information, Figure S2): these correspond to $0kl$ or $h0l$ (where $l \neq 2n$), which confirm the larger distortion from the parent tetragonal structure.

These problems with the structure determination of the La and Ce compounds by single-crystal X-ray diffraction prompted us to use transmission electron microscopy and selected area electron diffraction (SAED). The SAED patterns for the La-compound (Figure 5) confirmed the average body-centered orthorhombic symmetry (cell constants a = 4.3 Å, b = 4.4 Å, and c = 14.2 Å), which was inferred from the X-ray diffraction work (vide supra). Although to a much smaller extent, the lack of 4-fold symmetry can be detected for the Ce compound too. In both cases, reflections that do not belong to either the $I4_1/amd$ or $Imma$ space groups are clearly present: the SAED images in Figure 5 show well-defined satellite reflections of lower intensity. They appear to be arising from a commensurately modulated structure with a wave vector $\mathbf{q}$ (1/2, 1/2, 0), which should exist in the [110] direction.

This means the presence of a new basic reciprocal vector $a^{*\prime}$ = (1/2, 1/2, 0) × (a^*+b^*). In patterns taken along the $[1\bar{1}0]$ axis, more satellite reflections are visible, and they are suggestive of a higher-order commensurate modulation along this direction (Figure 5b). Such a modulation yields a new reciprocal vector $c^{*\prime}$ = (1/4, 1/4, 0) × (a^*+b^*), as represented in the right-hand-side of Figure 5b. These new vectors together with $b^{*\prime}$ (which is the unchanged c^*) account for a new modulated structure with orthorhombic symmetry; the new lattice parameters are determined as follows: $a' \sim 6.2$, $b' \sim 14.2$ Å, $c' \sim 12.4$ Å, in excellent agreement with the unit cell transformations discussed for Sm_4Ge_7 (Figure 4). In this sense, SAED confirms that the studied microcrystallites contain small domains of the La_4Ge_7 phase, which is isostructural with RE_4Ge_7 (RE = Pr, Nd, Sm). To brighten these satellite reflections, a small deviation (~2°) from the exact zone axis was used for the diffraction patterns shown in Figure 5. Nonetheless, the satellites are extremely weak, which likely indicates the low contents of these domains.

In addition to the commensurately modulated structure, the hallmarks of incommensurate modulation can also seen in the electron diffraction patterns: the electron beam focused on different regions of the "single-crystals" show a new kind of modulation, which has to be described using a (3 + 1)D (with a component $\mathbf{q}$ in the incommensurate dimension) network, as indexed in Figure 6. This is very clear from looking at the zone $[\bar{2}10]$ of the parent $Imma$ structure (Figure 6): it corresponds

dx.doi.org/10.1021/ic3021645 | Inorg. Chem. 2013, 52, 953−964

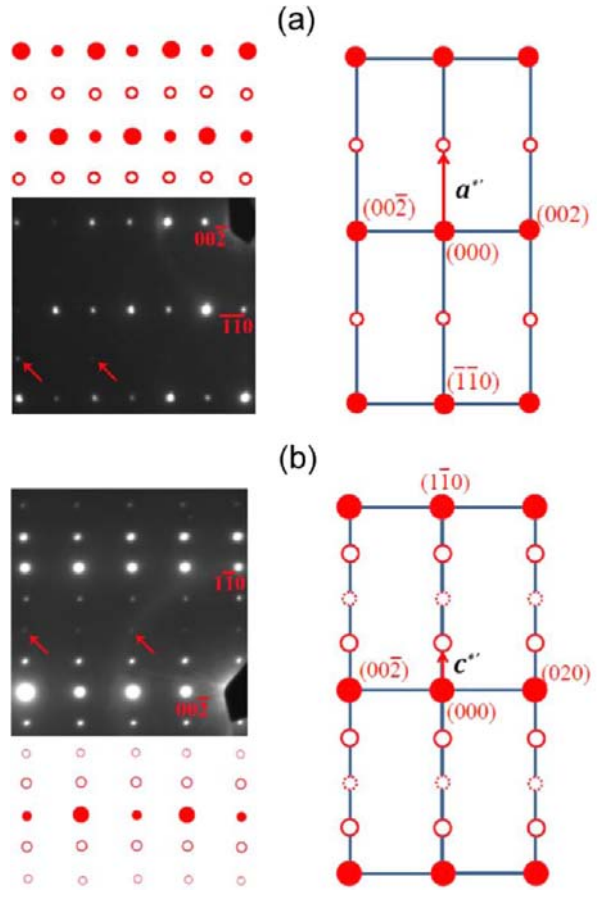

Figure 5. SAED patterns with schematic illustrations in right-hand for $LaGe_{2-x}$. The pattern shown in (a) is along the [1$\bar{1}$0] zone axis; the pattern shown in (b) is along the [110] zone axis of the parent *Imma* structure, respectively. The faint spots marked by the arrows in the left-hand side panels originate from the commensurate modulation. On the right-hand-side, solid circles represent first-order modulations, and dotted circles represent second-order modulations. The indexing agrees with the structural model in the space group $C222_1$.

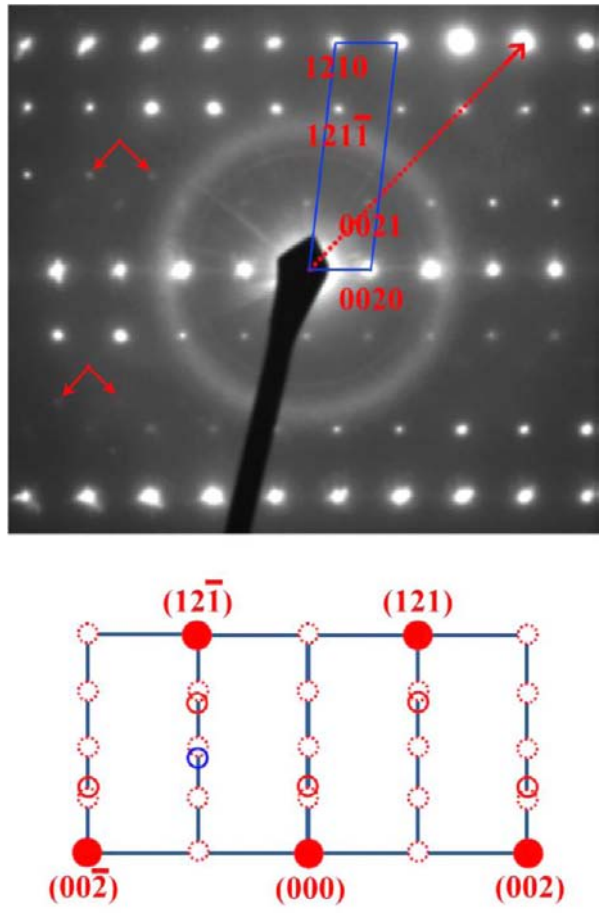

Figure 6. SAED pattern ([$\bar{2}$10] zone) for $LaGe_{2-x}$, along with a schematic illustration revealing reflections originating from the incommensurately modulated structure. The basic repeating unit in the subcell is outlined as a blue frame, and the dotted arrow indicates the modulation direction (127). The solid circles denote the spots from the incommensurate modulation; the dotted circles represent the spots from the commensurate modulation, respectively. The blue ovals represent the second-order reflections of incommensurate modulation, as marked with the small arrows.

to the [$\bar{3}$02] zone of the commensurate superstructure in space group $C222_1$. The reflections along the zone axis in the superstructure are simulated using the structural parameters from Sm_4Ge_7 (Tables 1 and 2). However, there are satellite reflections of incommensurate order, which are very close to the reflections originating from the commensurate ordering. Figure 7 shows the signature of an incommensurate modulation in a high-index [5$\bar{3}$1] zone (corresponding to zone [21$\bar{1}$] in the hypothetical commensurate La_4Ge_7 structure). From the comparison of the experimental and the simulated patterns for the substructures in *Imma* (I) and $I4_1/amd$ (II), it is evident that there are no extinct reflections, and that the strong spots match well the pattern I. The weaker-intensity spots appear to modulate the *Imma* pattern and are readily ascribed to the commensurate superstructure in space group $C222_1$ (III).

All of the above could be interpreted as if the incommensurate structure is the intermediate state between the fully ordered $LaGe_2$ with the α-$GdSi_2$ type structure and the La_4Ge_7 superstructure. Since the incommensurate domains are very small, their insufficient correlation length is the likely reason why they are not discerned from the single-crystal data. Nonetheless, the presence of incommensurate modulation can be surmised from the refinements for both the La and the Ce compounds, which could not produce satisfactorily results.

The coexistence of commensurately and incommensurately modulated structures is not without a precedent and has been previously reported in other compounds with complicated structures such as NiGeP[20] and $YbSi_{1.4}$,[21] where the incommensurate modulation is shown to bridge two perfectly commensurately modulated substructures, whereby the incommensurate structure arises from occupational modulation. Recent report in $CeSi_{2-x}$ suggested variations in the Si-vacancies as a cause of the on incommensurate modulation.[22] The incommensurate modulation can be therefore related to a topological disorder. These ideas appear to be applicable to the lanthanum germanide in question; its presumed incommensurately modulated structure calls for HAADF imaging at the atomic or nanoscale to confirm our reasoning.

Physical Properties. Temperature dependent direct current (DC) magnetization measurements were done for the RE_4Ge_7 compounds (*RE* = Ce−Nd, Sm), the La-analogue was not measured as the La^{3+} ion is not expected to a carry magnetic moment. The corresponding plots of the magnetization ($\chi = M/H$) as a function of temperature (T) are shown

dx.doi.org/10.1021/ic3021645 | *Inorg. Chem.* 2013, 52, 953−964

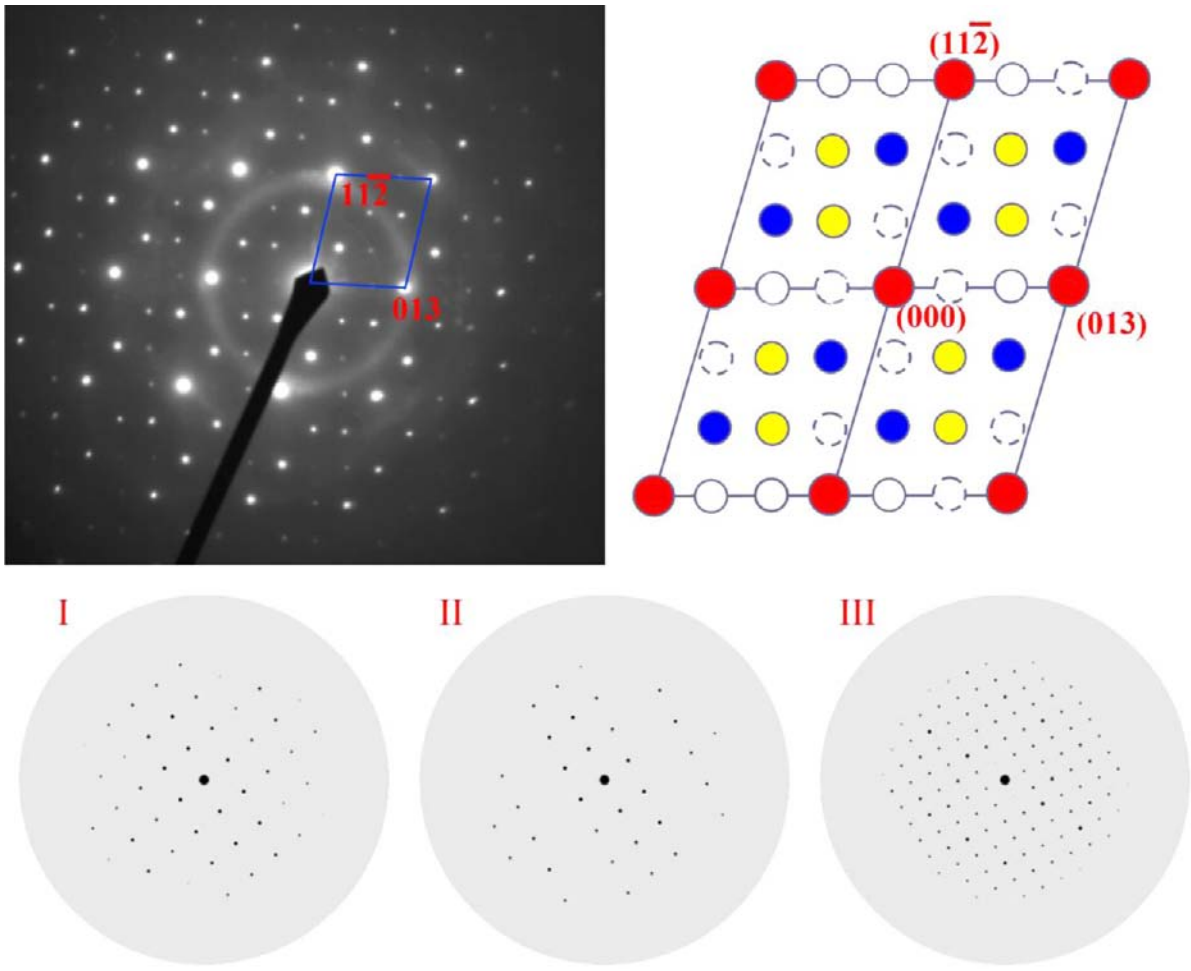

Figure 7. SAED pattern ([5$\bar{3}$1] zone) for $LaGe_{2-x}$. In the schematic diagram, blue and yellow dots represent the first-order and second-order satellite reflections, respectively. The solid circles denote the third-order satellite reflections and the dashed circles stand for absent satellites. The simulated patterns are for the [5$\bar{3}$1] zone of the α-$GdSi_2$ type structure (I); the [5$\bar{3}$1] zone of the α-$ThSi_2$ type structure (II); and the [21$\bar{1}$] zone of the Nd_4Ge_7 type structure (III).

in Figure 8. As can be seen from the cusp-like features in the data, the Ce and Sm compounds order antiferromagnetically below temperatures of T_N ~7 K and ~13 K, respectively. Nd_4Ge_7 exhibits ferromagnetism below the temperature of T_C ~4 K, determined from the midpoint of the jump in $d\chi/dT$. Although the magnetic transition of Pr compound does not appear completely finished down to 5 K, the very large susceptibility value suggests ferromagnetic ordering below T_C ~17 K.

Table 4 shows a compilation of selected magnetic data for the RE_4Ge_7 (RE = La–Nd, Sm) compounds, along with a few other $REGe_{2-x}$ phases with similar compositions. The $\chi^{-1}(T)$ data corresponding to Sm_4Ge_7 also revealed the existence of an anomaly around ~4 K, which is indicative of a consecutive magnetic transition and suggests two separated ordering temperature for the antiferromagnetic sublattices. The secondary transition is further supported by specific heat measurements (below). For all samples except Sm_4Ge_7, $\chi(T)$ data above T_N/T_C follow a Curie–Weiss law $\chi(T) = C/(T - \theta_p)$, where $C = N_A\mu_{eff}^2/3k_B$ is the Curie constant, and yields effective moments of $\mu_{eff} = 2.25(3)\ \mu_B/Ce^{3+}$, $\mu_{eff} = 3.48(4)\ \mu_B/Pr^{3+}$, and $\mu_{eff} = 3.62(4)\ \mu_B/Nd^{3+}$, in agreement with $\mu_{eff} = g[J(J+1)]^{1/2}$.[30] The Weiss temperatures θ_p are −22 K, 23 K, and 3 K, respectively, as expected for antiferromagnetically and ferromagnetically ordered compounds. The small effective moment on Sm results in fitting the magnetization data with the modified Curie–Weiss law $\chi(T) = \chi_0 + C/(T - \theta_p)$,[30] which takes into account also the van Vleck paramagnetic contributions to the magnetization, results in $\chi_0 = 8.8 \times 10^{-4}$ emu/mol and $\theta_p = -20$ K. The calculated effective moment of $\mu_{eff} = 0.64(3)\ \mu_B$ is slightly lower than expected for Sm^{3+} from the Hund's rules for the $[Xe]f^5$ configuration.[31] It should be noted that the magnetization data is subtly different from the data for the "presumed" defect-free $SmGe_2$ (α-$ThSi_2$ structure) which shows no long-range magnetic order down to 4.2 K.[29]

The magnetization is also clearly different from the $\chi(T)$ data for the α- and β-Sm_3Ge_5 polymorphs, exhibiting antiferromagnetic order at temperatures of 30 and 10 K, respectively. Evidently the change in Néel temperature should be correlated with the local structure caused by Ge deficiency instead of its concentration alone. The presence of a vacancy can relax around atoms, which is characterized by the shift of atoms toward the vacancy and changed local structure. According to the mean field theory,[32] the transition temperature can be related with a nearest neighbor exchange interaction as follows:

$$T_c = \frac{2ZJ_{ex}S(S+1)}{3k_B}$$

dx.doi.org/10.1021/ic3021645 | Inorg. Chem. 2013, 52, 953–964

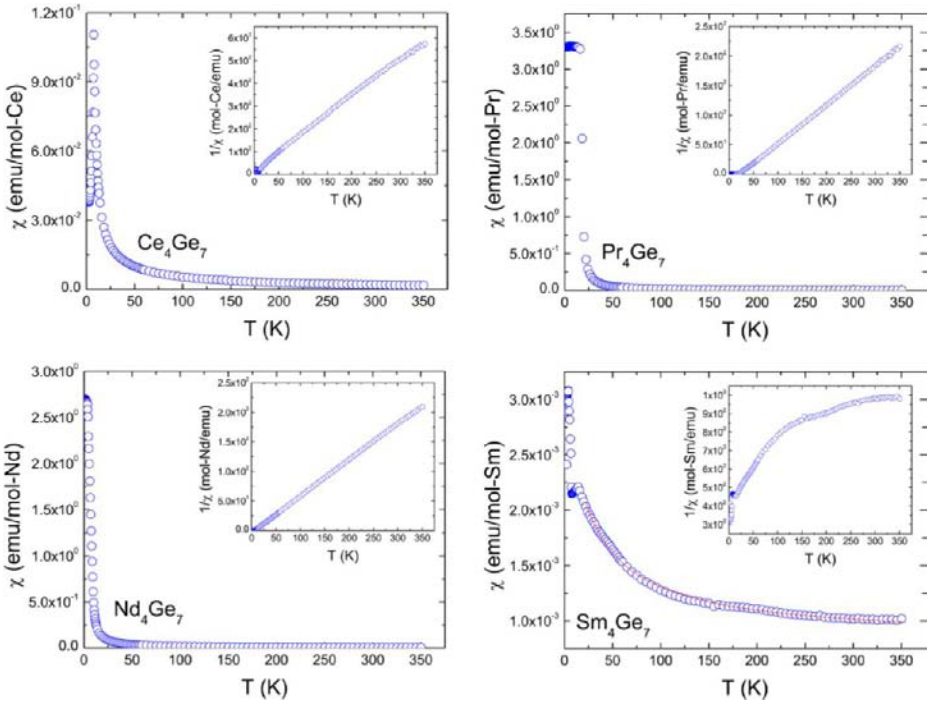

Figure 8. Temperature dependence of the magnetic susceptibility $\chi(T)$ for single-crystalline RE_4Ge_7 (RE = Ce, Pr, Nd, Sm) samples. The insets show the inverse susceptibility $\chi^{-1}(T)$. The presented data were obtained with the applied field perpendicular to the direction of the plates, but the ordering temperatures and the effective moments did not appear to depend on the orientation.

Table 4. Selected Magnetic Data for RE_4Ge_7 (RE = La−Nd, Sm) and Related Compounds

compound	structure type	T_N (K)	T_C (K)	θ_p (K)	ref.
$LaGe_{2-x}$	α-$GdSi_2$				23
$LaGe_{2-x}$	α-$GdSi_2$				24
La_4Ge_7	Nd_4Ge_7				*b*
$CeGe_{2-x}$	α-$GdSi_2$		4.5		24
$CeGe_{2-x}$	α-$GdSi_2$		7		25
$CeGe_{2-x}$	α-$GdSi_2$	7	4.3		26
$CeGe_{2-x}$	α-$ThSi_2$		7		27
$CeGe_{1.66}$	α-$ThSi_2$	7	6	15	28[a]
Ce_4Ge_7	Nd_4Ge_7	7		−22	*b*
$PrGe_{2-x}$	α-$ThSi_2$		19		23
$PrGe_{2-x}$	α-$ThSi_2$		19	22	29
$PrGe_{1.7}$	α-$ThSi_2$		17		27[a]
Pr_4Ge_7	Nd_4Ge_7		17	23	*b*
$NdGe_{2-x}$	α-$ThSi_2$		3.6		23
$NdGe_{2-x}$	α-$ThSi_2$		3.6	7	29
Nd_4Ge_7	Nd_4Ge_7		4	3	*b*
$SmGe_{2-x}$	α-$ThSi_2$			−10	29
Sm_4Ge_7	Nd_4Ge_7	13, 4		−20	*b*
α-Sm_3Ge_5	α-Y_3Ge_5	30		−8.4	4a
β-Sm_3Ge_5	β-Y_3Ge_5	10		−9.9	4a

[a]Only in these publications the substoichiometry of the studied samples have been determined. [b]This work.

where J_{ex} is the exchange energy, Z is the number of magnetic nearest neighbors, k_B is Boltzmann constant, and S is the total spin angular momentum. The relevant Sm−Sm distances are very close among the three samarium germanides, so J_{ex} and S should be similar. The value of Z can be obtained as following: 6 for Sm in α-Sm_3Ge_5; 4 for Sm1 and 2 for Sm2 in β-Sm_3Ge_5, 5 for Sm1, 4 for Sm3, and 2 for Sm2 in Sm_4Ge_7. Evidently it predicts the highest ordering temperature for α-Sm_3Ge_5 and lowest ordering temperature for β-Sm_3Ge_5.

The (co)existence of commensurate and incommensurate modulated structures, very likely, leads to complex magnetic ordering in such compounds, as it can be inferred from glancing over the multitude of T_N and T_C values in Table 4. Therefore, we conducted zero field-cooled (ZFC) and field-cooled (FC) measurements on our single-crystalline specimens. Since the measurements for the Ce, Nd, and Sm compounds did not show any visible difference, they are not presented. The ZFC-FC measurement for Pr_4Ge_7 reveals a spin-glass-like behavior, as shown in Figure 9.

Although a mixture of ferromagnetic and antiferromagnetic states can also produce such behavior in ZFC-FC measurement, the field dependent magnetization measurements at 2 K

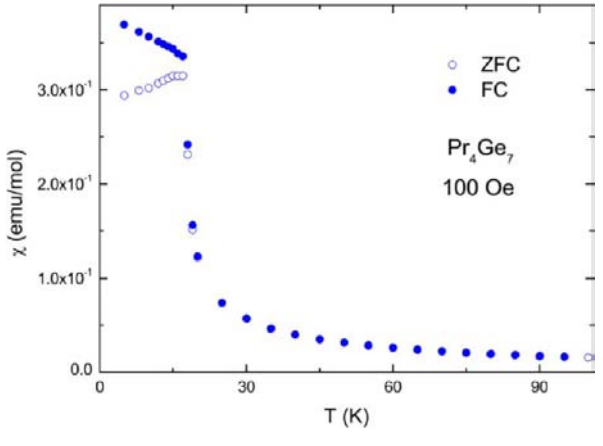

Figure 9. Zero-field cooled (ZFC) and field-cooled (FC) curves for Pr_4Ge_7.

dx.doi.org/10.1021/ic3021645 | *Inorg. Chem.* 2013, 52, 953−964

(shown in Figure 10) do not show any trace of antiferromagnetism, because the rapid saturation at about 2.5 μ_B is very close

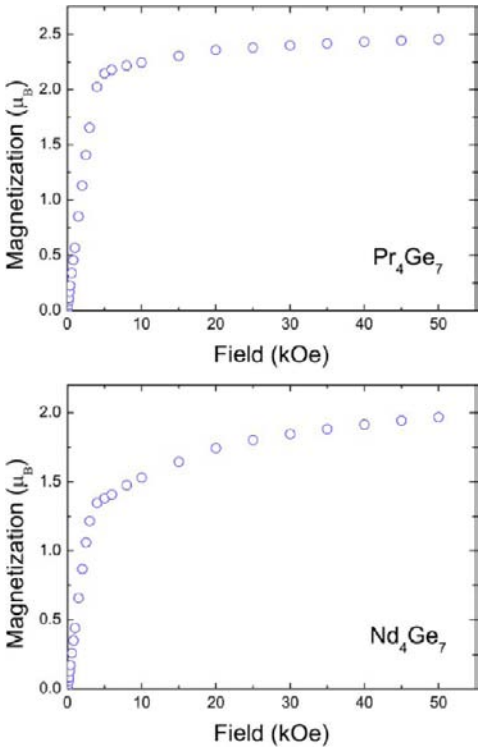

Figure 10. Magnetization (M) as a function of the applied field for Pr_4Ge_7 and Nd_4Ge_7.

to that of other ferromagnetic Pr−Ge compounds.[27,29] It is very surprising to observe spin-glass-like behavior in such a binary system, which calls for a more detailed investigation. Compared with Pr_4Ge_7, the saturation of the Nd moments in Nd_4Ge_7 (at ca. 2.1 μ_B) occurs at a slower rate. For $CeGe_{2-x}$ samples (reported with the α-$GdSi_2$ type structure), previous magnetic susceptibility studies have revealed that when $0 < x < 0.3$, two magnetic transitions are observed, an antiferromagnetic transition at T_N = 7 K and a ferromagnetic transition at T_C = 4.3 K.[26] At higher vacancy concentrations, only the antiferromagnetic state has been suggested to exist.[23] Yet, another report on a phase with established composition $CeGe_{1.66}$ has found it to undergo antiferromagnetic ordering at 7 K and ferromagnetic ordering at 6 K, respectively.[28] Our Ce_4Ge_7 crystals show only one ordering transition at 7 K. Again the change in magnetic transition should be correlated with the induced local structure instead of only the concentration of Ge deficiency. Lastly, samples of $LaGe_{2-x}$ (reported as $LaGe_2$)[24] have been suggested to be superconductors below 1.5−2.2 K, an observation which could not be confirmed or refuted since we were unable to measure our La_4Ge_7 crystals to sufficiently low temperatures.[33]

Calorimetry and resistivity data taken on single crystals along the direction of the plate are shown in Figures 11 and 12. The cusp-like features in the C_p/T vs T plots as depicted in the insets are consistent with the respective ordering temperatures obtained from the magnetization data. It is also worthwhile to mention that the specific heat asymptotically reaches a value of 275 J/mol·K at high temperatures close to that expected according the Dulong−Petit law.[34] The C_p/T vs T data for Sm_4Ge_7 also provides evidence for the possible consecutive ordering at ∼4 K. Electrical resistivity measurements show that the compounds exhibit metallic behavior in the whole temperature range; at the lowest temperatures $\rho(T)$ dependence can be fitted to $\rho(T) = \rho_0 + A \cdot T^2$. The T^2 dependence suggests the dominant role of electron−electron scattering in this temperature region. Closer inspection of the low temperature data shows abrupt changes of the slope at

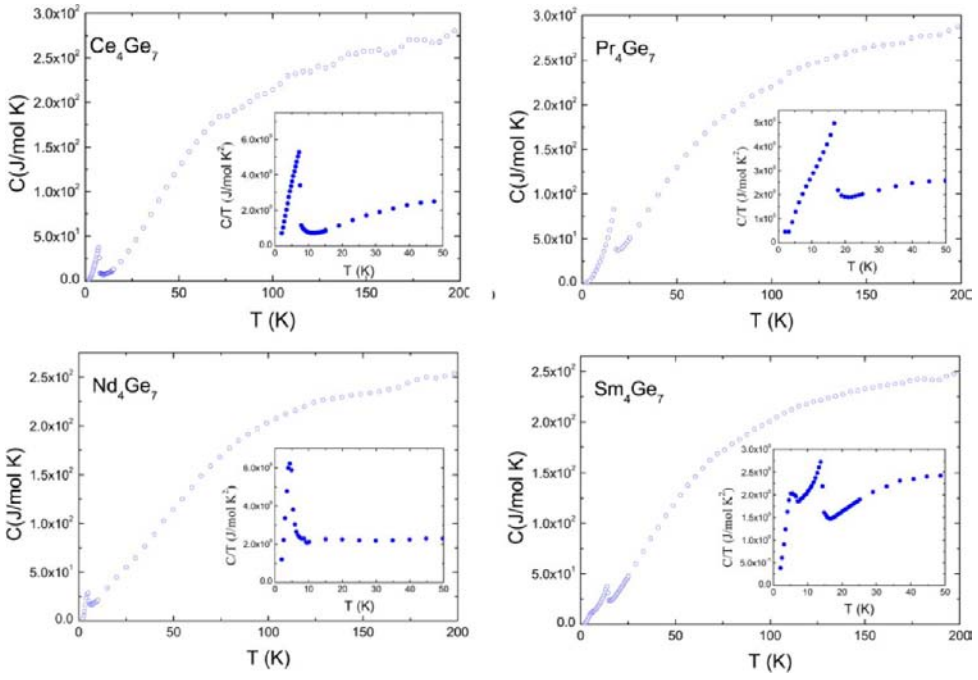

Figure 11. Temperature dependence of the specific heat for the RE_4Ge_7 (RE = Ce, Pr, Nd, Sm) compounds. In the insets, the data are represented in the form C_p/T vs T.

dx.doi.org/10.1021/ic3021645 | Inorg. Chem. 2013, 52, 953−964

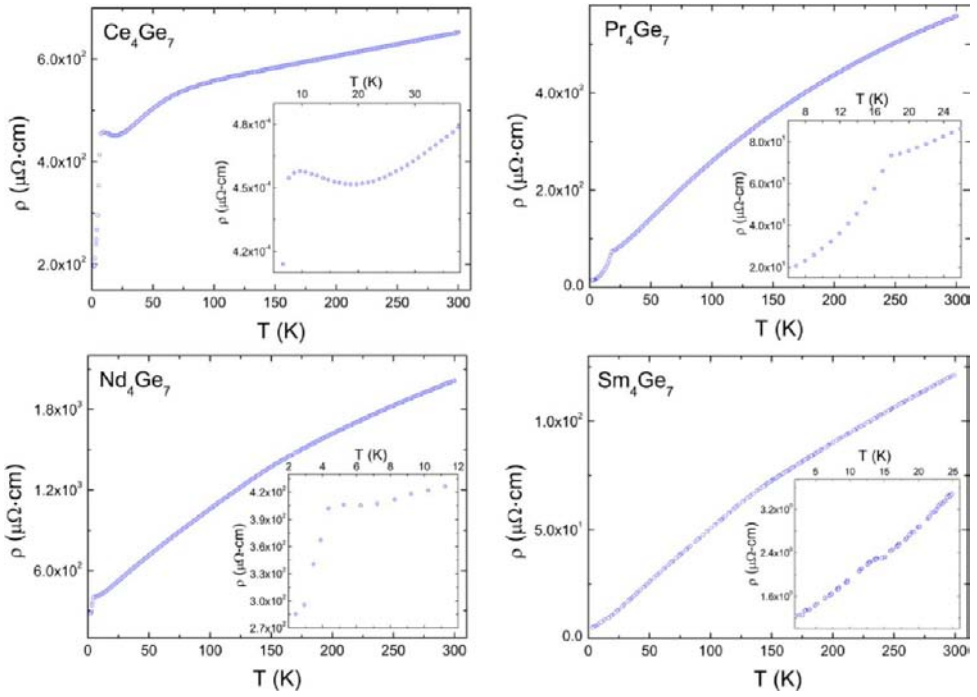

Figure 12. Four-probe electrical resistivity as a function of the temperature for RE_4Ge_7 (RE = Ce, Pr, Nd, Sm). Insets show magnified views at low temperatures. Data were collected on both cooling and heating and show no differences.

temperatures coinciding with the ordering temperatures found by magnetic susceptibility measurements (Table 4).

For the Ce compound, above about 100 K, $\rho(T)$ displays a linear dependence on T, but the low temperature regime is markedly different than the rest of the samples. First, the resistivity is significantly higher, and second, no kink in the $\rho(T)$ curve is observed near the magnetic ordering point; instead the resistivity reaches a valley and then drops. This is suggestive of a transition in the scattering mechanism (from electron−phonon/impurities to electron−electron). It is most likely due to the enhanced role of 4f electrons in the conductivity (i.e., heavy-fermion behavior). The higher resistivity likely stems from the intrinsic structure or from scattering due to 4f electrons (very close to the Fermi surface).

Such behavior is a typical feature of Kondo systems, as observed in other Ce-based compounds, such as $CeNiSb_3$,[35] $CeSn_{0.7}Sb_2$.[36] It is also in agreement with the enhanced negative Curie temperature and the correspondence between magnetic ordering and resistivity maximum. The low temperature power law $\rho-\rho_0 = AT^n$ can be employed to fit the resistivity from about 4 K to the magnetic ordering temperature (to avoid the possible influence of In flux), which yields the following values: A = 6.3(2) and n = 2.0(1). On the basis of the empirical Kadowaki−Woods relation ($A/\gamma^2 = 1 \times 10^{-5}$ $\mu\Omega$·cm(mol·K/mJ)^2),[37] the Sommerfeld coefficient γ can be estimated to be ~250 mJ/mol·K. It is close to the values of many heavy-fermion systems,[38] implying the existence of a Fermi-liquid ground state in the compound in question. The sharp drop of the resistivity at low temperature has also been observed in several Ce-based heavy-fermion compounds, hinting at superconducting transitions in these compounds.[39]

CONCLUSIONS

Crystals of RE_4Ge_7 (RE = La−Nd, Sm) have been grown using the In-flux technique and structurally characterized by X-ray and electron diffraction. Their structures represent superstructures of $REGe_{2-x}$ with the α-$ThSi_2$ or α-$GdSi_2$ type structures, where x = 1/4. The structures are realized through the long-range order of vacant Ge positions. Further structural analysis reveals the coexistence of commensurate and incommensurate modulations in the La and Ce compounds. The incommensurately modulated structure of $REGe_{2-x}$ (RE = La, Ce) needs HAADF-HRTEM imaging to be fully understood, and such investigations are expected to commence in near future.

On the basis of magnetization, resistivity, and heat-capacity measurements on single-crystals, ferromagnetic and antiferromagnetic magnetic ordering have been confirmed in the studied samples. Some of the gathered data do not agree with decades-old reports on predominantly polycrystalline materials with poorly defined composition, calling for more detailed studies of the magnetic structures. We can argue that the low-temperature properties of the RE_4Ge_7 compounds are clearly rooted in the intricate structures. In the examples where very high degree of crystallographic order is apparent, that is, RE_4Ge_7 (RE = Pr, Nd, Sm), resistivity data clearly show that magnetic ordering does reduce the resistivity, although the magnitude of the effect is different. For the La-compound, in the absence of spin-fluctuation effects, the $\rho(T)$ behavior must be correlated with the local structure and a probable transition between commensurate and incommensurate modulations could be suggested. For the Ce compound, a combination of the above, in addition to the probable heavy-fermion behavior (a hallmark of many Ce-containing compounds) must be discussed in attempts to understand its properties.

ASSOCIATED CONTENT

Supporting Information

Tables with the data collection and structure refinement parameters using three structural models (α-$ThSi_2$, α-$GdSi_2$, and Nd_4Ge_7); tables with atomic coordinates and equivalent

dx.doi.org/10.1021/ic3021645 | Inorg. Chem. 2013, 52, 953−964

displacement parameters for α-$ThSi_2$, α-$GdSi_2$ structure type refinements; tables with interatomic distances in Pr_4Ge_7 and Nd_4Ge_7; figures showing experimental and simulated powder XRD patterns; zone images from single-crystal X-ray diffraction. This material is available free of charge via the Internet at http://pubs.acs.org.

AUTHOR INFORMATION

Corresponding Author

*Fax: (302) 831-6335. E-mail: bobev@udel.edu.

Author Contributions

The manuscript was written through contributions of all authors. All authors have given approval to the final version of the manuscript.

Notes

The authors declare no competing financial interest.

ACKNOWLEDGMENTS

S.B. acknowledges financial support from the National Science Foundation through Grant DMR-0743916 (CAREER). P.H.T. wishes to thank the University of Delaware for the University Graduate Fellowship and the International Centre for Diffraction Data (ICDD) for the Ludo Frevel Crystallography Scholarship. Work at LANL was done under the auspices of the U.S. DOE.

REFERENCES

(1) (a) Guloy, A. M.; Corbett, J. D. *Inorg. Chem.* **1991**, *30*, 4789. (b) Schlottmann, P. *J. Appl. Phys.* **2002**, *91*, 8114. (c) Bobev, S.; Bauer, E. D.; Thompson, J. D.; Sarrao, J. L.; Miller, G. J.; Dronskowski, R. *J. Solid State Chem.* **2004**, *177*, 3545. (d) Morozkin, A. V.; Seropegin, Yu. D. *J. Alloys Compd.* **2004**, *365*, 168. (e) Zaharko, O.; Schibinger-Papamantellos, P.; Ritter, C.; Janssen, Y.; Brueck, E.; de Boer, F. R.; Buschow, K. H. J. *J. Phys.: Condens. Matter* **1998**, *10*, 2881. (f) Salamakha, P. S.; Sologub, O. L.; Demchenko, P.; Righi, L.; Bocelli, G. *J. Alloys Compd.* **2001**, *315*, 1. (g) Budnyk, S.; Weitzer, F.; Kubata, C.; Prots', Yu.; Aksel'rud, L. G.; Schnell, W.; Hiebl, K.; Nesper, R.; Wagner, F. R.; Grin', Yu. *J. Solid State Chem.* **2006**, *179*, 2329.

(2) (a) Zan, J. A.; Yuen, T.; Lin, C. L.; Huang, X. Y.; Li, J. *J. Appl. Phys.* **2003**, *93*, 8340. (b) Lambert-Andron, B.; Boutarek, N.; Pierre, J.; Madar, R. *J. Alloys Compd.* **1994**, *203*, 1. (c) Morozkin, A. V.; Stupnikov, V. A.; Nikiforov, V. N.; Imaoka, N.; Morimoto, I. *J. Alloys Compd.* **2006**, *415*, 12. (d) Oleksyn, O.; Schobinger-Papamantellos, P.; Ritter, C.; de Groot, C. H.; Buschow, K. H. J. *Phys. B* **1997**, *234*, 652.

(3) (a) Lambert-Andron, B.; Pierre, J.; Chenevier, B.; Madar, R.; Boutarek, N.; Rodriguez-Carvajal, J. *J. Phys.: Condens. Matter* **1994**, *6*, 8725. (b) Lambert-Andron, B.; Houssay, E.; Madar, R.; Pierre, J.; Auffret, S. *J. Less-Common Met.* **1990**, *167*, 53.

(4) (a) Tobash, P. H.; Lins, D.; Bobev, S.; Hur, N.; Thompson, J. D.; Sarrao, J. L. *Inorg. Chem.* **2006**, *45*, 7286. (b) Tobash, P. H.; Bobev, S.; Thompson, J. D.; Sarrao, J. L. *J. Alloys Compd.* **2009**, *488*, 533.

(5) Massalski, T. B., Ed.; *Binary Alloys Phase Diagrams*; ASM International: Materials Park, OH, 1990.

(6) (a) Canfield, P. C.; Fisk, Z. *Philos. Mag. B* **1992**, *65*, 1117. (b) Kanatzidis, M. G.; Pöttgen, R.; Jeitschko, W. *Angew. Chem., Int. Ed.* **2005**, *44*, 6996. (c) Tobash, P. H.; Lins, D.; Bobev, S.; Lima, A.; Hundley, M. F.; Thompson, J. D.; Sarrao, J. L. *Chem. Mater.* **2005**, *17*, 5567 ; Caution: while advantageous to overcome kinetic obstacles, employing a flux, however, can lead to phase equilibria which do not reflect the thermodynamics of the binary phase diagram.

(7) (a) Venturini, G.; Ijjaali, I.; Malaman, B. *J. Alloys Compd.* **1999**, *289*, 168. (b) Shcherban, O.; Savysyuk, I.; Semuso, N.; Gladyshevskii, R.; Cenzual, K. *Chem. Met. Alloys* **2009**, *2*, 115.

(8) Morozkin, A. V. *J. Alloys Compd.* **1999**, *287*, 185.

(9) (a) Schobinger-Papamantellos, P.; Buschow, K. H. J. *J. Magn. Magn. Mater.* **1989**, *82*, 99. (b) Salamakha, P. S.; Sologub, O. L.; Demchenko, P.; Righi, L.; Bocelli, G. *J. Alloys Compd.* **2001**, *315*, 1. (c) Grytsiv, A. V.; Kaczorowski, D.; Leithe-Jasper, A.; Rogl, P.; Potel, M.; Noel, H.; Pikul, A.; Velikanova, T. *J. Solid State Chem.* **2002**, *165*, 178.

(10) Christensen, J.; Lidin, S.; Malaman, B.; Venturini, G. *Acta Crystallogr., Sect. B* **2008**, *64*, 272.

(11) Lide, D. R., Ed.; *CRC Handbook of Chemistry and Physics*; 83rd ed.; CRC Press: Boca Raton, FL, 2002.

(12) *SMART*; Bruker Analytical X-ray Systems, Inc.: Madison, WI, 2003.

(13) *SAINT NT*, Version 6.45; Bruker Analytical X-ray Systems, Inc.: Madison, WI, 2003.

(14) Sheldrick, G. M. *SADABS*; University of Göttingen: Göttingen, Germany, 2003.

(15) Sheldrick, G. M. *SHELXTL*; University of Göttingen: Göttingen, Germany, 2001.

(16) Villars, P., Calvert, L. D., Eds.; *Pearson's Handbook of Crystallographic Data for Intermetallic Phases*, 2nd ed.; ASM International: Materials Park, OH, 1991.

(17) (a) Schobinger-Papamantellos, P.; Buschow, K. H. J. *J. Less-Common Met.* **1983**, *111*, 125. (b) Bobev, S.; You, T.-S.; Suen, N.-T.; Saha, S.; Greene, R.; Paglione, J.-P. *Inorg. Chem.* **2012**, *51*, 620.

(18) (a) Oleksyn, O.; Bodak, O., I. *J. Alloys Compd.* **1994**, *210*, 19. (b) Tobash, P. H.; DiFilippo, G.; Bobev, S.; Hur, N.; Thompson, J. D.; Sarrao, J. L. *Inorg. Chem.* **2007**, *46*, 8690.

(19) Pauling, L. *The Nature of the Chemical Bond*; Cornell University Press: Ithaca, NY, 1960.

(20) (a) Larsson, A. K.; Garcia, F. J.; Withers, R .L. *J. Solid State Chem.* **2007**, *180*, 1093. (b) Vincent, R.; Pretty, S. F. *Philos. Mag., A* **1986**, *53*, 843.

(21) Kubata, C.; Krumeich, F.; Worle, M.; Nesper, R. *Z. Anorg. Allg. Chem.* **2005**, *631*, 546.

(22) Leisegang, T.; Meyer, D. C.; Doert, T.; Zahn, G.; Weissbach, T.; Souptel, D.; Behr, G.; Paufler, P. *Z. Kristallogr.* **2005**, *220*, 128.

(23) Matthias, B. T.; Corenzwit, E.; Zachariasen, W. H. *Phys. Rev.* **1958**, *112*, 89.

(24) Satoh, T.; Asada, Y. *J. Phys. Soc. Jpn.* **1969**, *27*, 1463.

(25) Yashima, H.; Satoh, T.; Mori, H.; Watanabe, D.; Ohtsuka, T. *Solid State Commun.* **1982**, *41*, 1.

(26) Lin, C. L.; Yuen, T.; Riseborough, P.; Huang, X. Y.; Li, J. *J. Appl. Phys.* **2002**, *91*, 8117.

(27) Boutarek, N.; Pierre, J.; Lambertandron, B.; Leritier, P.; Madar, R. *J. Alloys Compd.* **1994**, *204*, 251.

(28) Nakano, T.; Hedo, M.; Uwatoko, Y. *Phys. B* **2005**, *359*−*361*, 284.

(29) Sekizawa, K. *J. Phys. Soc. Jpn.* **1966**, *21*, 1137.

(30) Smart, J. S. *Effective Theories of Magnetism*; Saunders: Philadelphia, PA, 1996.

(31) Stewart, A. M. *Phys. Rev. B* **1972**, *6*, 1985.

(32) Kittel, K. *Introduction of Solid State Physics*, 5th ed.; Wiley: New York, 1976.

(33) For the La-compound (see Supporting Information), resistivity measurements down to 2 K do not provide an affirmative answer to the question of whether the material is an intrinsic superconductor. The downturn in the plot, like in the case of the Ce-compound, is likely due to traces of In (flux, T_C = 3.4 K). We also note that the $\rho(T)$ behavior above 20 K is nearly linear, and the resistivity values are lower than that of the Ce-counterpart, which lands support of the speculation that the 4f-electrons are the reason for the change in scattering mechanism (and the nonlinear temperature dependence) of the Ce-based material.

(34) Landau, L. D.; Lifshitz, E. M. *Statistical Physics Pt. 1. Course in Theoretical Physics*, 3rd ed.; Pergamon Press: Oxford, U.K., 1980; p 193.

(35) Sidorov, V. A.; Bauer, E. D.; Lee, H.; Nakatsuji, S.; Thompson, J. D.; Fisk, Z. *Phys. Rev. B* **2005**, *71*, 094422.

(36) Deakin, L.; Ferguson, M. J.; Sprague, M. J.; Mar., A.; Shama, R. D.; Jones, C. H. W. *J. Solid State Chem.* **2002**, *164*, 292.

(37) Kadowaki, K.; Woods, S. B. *Solid State Commun.* **1986**, *58*, 307.

(38) (a) Macaluso, R. T.; Millican, J. N.; Nakatsuji, S.; Lee, H. O.; Carter, B.; Moreno, N. O.; Fisk, Z.; Chan, J. Y. *J. Solid State Chem.* **2005**, *178*, 3547. (b) Medina, A. N.; Hayashi, M. A.; Cardoso, L. P.; Gama, S.; Gandra, F. G. *Phys. Rev. B* **1998**, *57*, 5900. (c) Van Daal, H. J.; Buschow, K. H. J. *Phys. Status Solidi* **1970**, *3*, 853.
(39) (a) Petrovic, C.; Pagliuso, P. G.; Hundley, M. F.; Movshovich, R.; Sarrao, J. L.; Thompson, J. D.; Fisk, Z.; Monthoux, P. *J. Phys.: Condens. Matter* **2001**, *13*, L337. (b) Petrovic, C.; Movshovich, R.; Jaime, M.; Pagliuso, P. G.; Hundley, M. F.; Sarrao, J. L.; Fisk, Z.; Thompson, J. D. *Europhys. Lett.* **2001**, *53*, 354.